*FUDMA Journal of Sciences (FJS)*
*ISSN online: 2616-1370*
*ISSN print: 2645 - 2944*
*Vol. 9 No. 9, September, 2025, pp 287 – 297*
*DOI: https://doi.org/10.33003/fjs-2025-0909-3785*

# EMPIRICAL AND SPATIAL RELATION BETWEEN MAGNETIC AND RADIOMETRIC SURVEY OVER MICA SCHIST AREA, OGUN STATE, NIGERIA

***[1]Ogunsanwo, Fidelis Olatoyosi, [2]Mustapha, Amidu Olalekan, [3]Ozebo, Vitalis Chidi, [2]Okeyode, Itunu Comfort, [1]Ayanda, Jacob Dele and [1]Sanni, Kikelomo Racheal**

[1]Physics Department, Tai Solarin University of Education, Ijagun, Ogun State, Nigeria
[2]Physics Department, Federal University of Agriculture, Abeokuta, Ogun State, Nigeria.
[3]Physics Department, University of Lagos, Akoka, Lagos State, Nigeria.

*Corresponding authors' email: godif07@yahoo.com

## ABSTRACT

The integration of magnetic and radiometric methods has received limited attention in mica schist terrains, despite their complementary sensitivity to lithological and geochemical variations. This study addresses this gap by jointly applying magnetic measurements and soil radiometric analyses over the mica deposit zone of Area J4, Ogun State, Nigeria. The magnetic surveys capture variations in rock magnetization, while radiometric surveys quantify radioelement concentrations (U, Th, K), and their empirical integration enables a more robust characterization of subsurface heterogeneity. The results demonstrate strong positive correlations between magnetic intensity and radioelement concentrations, with regression models confirming direct proportional relationships. This finding highlights the predictive capacity of integrated geophysical datasets, whereby one survey can be used to infer or validate anomalies detected by the other. Spatial contour mapping further delineated coincident magnetic–radiometric anomalies, strengthening the case for exploration targets associated with radioelement-rich mineralization. Beyond local outcomes, this study emphasizes the broader value of multi-method geophysics in mineral exploration. By establishing empirical relationships between datasets, interpretational ambiguities are reduced, anomaly discrimination is improved, and the efficiency of resource targeting is enhanced. Such integrative approaches are particularly relevant in complex Precambrian terrains, where single-method surveys may overlook subtle but economically significant signals. Methodological limitations include the restricted survey coverage and focus on near-surface soil samples, which may not fully represent deeper lithological variations. Conclusively, this study have demonstrates the scientific and practical relevance of integrating magnetic and radiometric methods as a predictive framework for mineral exploration and geophysical mapping.

**Keywords**: Radioelement, Model, Inferential, Anomalous, Spatial

## INTRODUCTION

Geophysical methods remain indispensable in mineral exploration because they provide indirect but reliable insights into the subsurface without the expense of extensive drilling (Shirazy et al 2020). Among these methods, magnetic and radiometric surveys are widely applied, as they respond to different but often complementary physical properties of rocks. Magnetic surveys measure variations in the Earth's magnetic field caused by contrasts in rock magnetization, which can delineate lithological units, structural features, and mineralization zones (Blakely, 1995; Hinze et al., 2013). Radiometric surveys, on the other hand, quantify the natural gamma radiation emitted by uranium (U), thorium (Th), and potassium (K), which serve as geochemical markers of lithology, alteration, and mineralization processes (Dickson and Scott, 1997; Minty, 1997).

A wide range of lithological units within mineralized zones including; bitumen, phosphate, tantalite, peat, granites, and gold, have been investigated using magnetic and radiometric methods, with several studies establishing geological and mathematical relationships between their geophysical responses (Ammar, 1988; Saunders et al., 1993; Fouad et al., 1996; El-Sadek, 2002; Youssef, 2016; Elhusseiny, 2022; Ogunsanwo et al., 2023). Beyond these, integrated magnetic–radiometric approaches have also been applied in the exploration of specific mineral deposits such as copper-bearing zones (Ammar et al., 1993), peat and chalk (Beamish, 2013), kimberlite (Ramadass et al., 2015), and gold (Airo, 2007; Boadi et al., 2013; Ohioma et al., 2017).

Although both methods have demonstrated effectiveness when applied independently, fewer studies have systematically examined their empirical and spatial interrelationships, particularly within mica schist terrains. Mica-rich schists are of geological and economic interest due to their mineral associations, including pegmatites and radioelement-bearing phases. However, in such terrains, the potential correlation between magnetic responses and radiometric signatures remains poorly understood. Most previous studies in Precambrian basement complexes of Nigeria have focused on either magnetic or radiometric datasets in isolation, leaving a knowledge gap in their integrated application for mineral prospecting. However, integrating both through empirical relationships allows for cross-validation and a more robust understanding of subsurface geology. For instance, lithological units enriched in potassium-bearing minerals may also display corresponding magnetic signatures due to their mineralogical associations. Similarly, anomalous zones in radioelement concentration can be better constrained and interpreted when correlated with magnetic intensity variations.

The novelty of this study lies in showing that integrating magnetic and radiometric interpretations within mica schist terrains can minimize geophysical uncertainties and significantly improve the delineation of radioelement-associated mineralization. Hence, this study addresses this gap by investigating the empirical and spatial relationships between magnetic intensity and radioelement concentrations in the mica schist area of Ogun State, southwestern Nigeria. The primary objective is to quantify the correlation, map the

anomalies and establish regression models between magnetic intensity and the concentration of radioactive elements within the mica-rich zone.

## MATERIALS AND METHODS

### Geological Description of the Study Area

Seven bedrock compositions were identified with the study area such that the traverses cut across the lithological units. The two traverses T1 and T2 were found to be underlain by five rock units, namely; Banded gneiss, migmatite, clay and sand, biotite and granodiorite, undifferentiated schist (Figure 1). The study area has wider representation and coverage of crystalline intrusive rock intermediate by small portion of sand and clay. According to Ayanda et al (2006); Ayanda and Popoola, (2018), the area has been confirmed to be dominated with mica deposits. Mica is a true reflection and end product of biotite and gneiss schist which has been metamorphosis. Geochemical analysis suggests that the schist likely originated from the metamorphism of shale. Modal composition shows mica schist area must reflect the assemblages of some of the minerals such as quartz, plagioclase, microcline, biotite , muscovite and hornblende (Alaku et al 2017; Usman and Ibrahim, 2017). The presence of those mineral grains gives mica schist its distinctive flaky texture, often appearing as shiny flecks within the rock. The geological unit called undifferentiated schist has been identified to be sometimes quartz mica schist when associated probably with intense grades of metamorphism (Odokuma-Alonge and Dibani, 2022; Abdus-salam et al 2020).

The rock units appeared in a distinct layer pattern such that biotite and granodiorite was observed in the NW segment followed by undifferentiated schist trending N – S, while migmatite was found in the Eastern part trending Southward. Clay and sand unit was found to intermediate between banded gneiss and migmatite. Granite gneiss was found to be embedded within banded gneiss while quartz feldspathic schist was found in the NE section underlain by migmatite and bounded by sand and clay.

### Survey Design, Instrumentation, and Data Corrections

Magnetic and radiometric surveys were designed to run along coincident traverses, ensuring spatial comparability between datasets. Traverses were oriented across the dominant geological strike, with a line spacing of 20 m and regular station intervals to provide sufficient resolution for mapping subtle lithological variations. A magnetic base station was established at a magnetically quiet location to record diurnal variations, while for radiometric measurement, soil samples were collected along the traverses at the depth of about 7cm from the top soil. The samples collected were taken at each point of magnetic survey with the aid of global positioning system (GPS).

### Magnetic Survey

The two traverses were obtained such that T1 and T2 are adjacent to each other, that is, one in the upper part while the second in the lower section of the study area. Magnetic data were acquired using a proton precession magnetometer (PPM), which measures the total intensity of the geomagnetic field with a sensitivity of 0.1 nT and orientation-independent accuracy. The instrument records proton precession frequencies, providing absolute field strength values unaffected by heading errors. Corrections applied included despiking, diurnal variation removal using base-station data, and subtraction of the International Geomagnetic Reference Field (IGRF) to obtain residual anomalies. Leveling along tie-lines, micro-leveling to reduce line-to-line noise, and filtering were also applied before gridding and anomaly mapping.

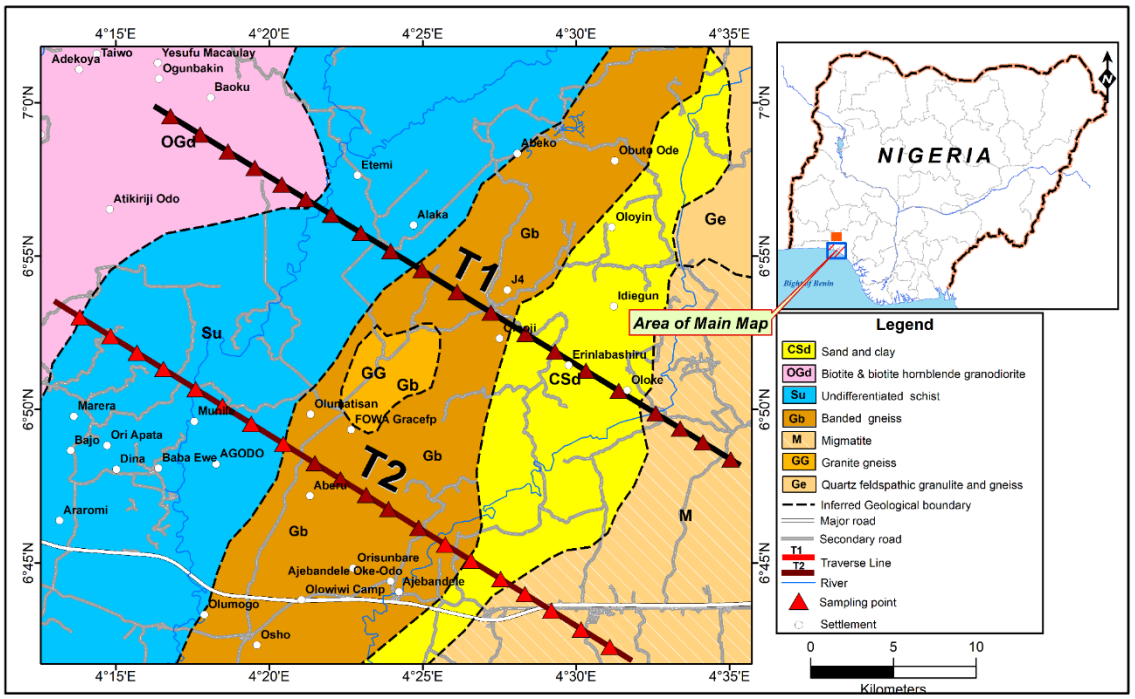


Figure 1: Geological Map of J4 Forest Reserve with Traverse Line

**Radiometric Survey and Analysis**

A total of 30 samples were collected with 15 each along the traverse at 20m spacing. A total ground distance of 0 – 300 m was covered for a single traverse. The samples were collected in a polythene bag which was sealed. The samples were then prepared for radiometric analysis by sundried, reduce to granule and sieve with a mesh such that 250g of each sample was packed into a plastic container and sealed for 24 days in order to attain secular equilibrium. The samples were analyzed at the Radiation Laboratory of the National Institute of Radiation Protection Centre, University of Ibadan, using a gamma-ray spectrometer equipped with a 2" × 2" Sodium Iodide (NaI) detector doped with Thallium, connected to a Digibase multichannel analyzer. The spectrometer provides spectral resolution of ~7–8% at 662 keV, with windowed outputs 1.37–1.57 MeV for K, 1.66–1.86 MeV for eU, and 2.41–2.81 MeV for eTh. Data corrections included background subtraction, energy calibration against reference sources, spectral stripping to remove window overlap, and dead-time adjustments. Radon and soil moisture effects were minimized by careful timing of measurements and field quality control.

**Radiometric Variable Conversion**

The radioelements were obtained in Becquerel per kilogram ($Bqkg^{-1}$) for uranium, thorium and potassium. For geological survey, the conventional unit is part per million (ppm), percent (%) and milligram per kilogram ($mgkg^{-1}$). In this study, ppm was adopted for equivalent uranium and equivalent thorium while percent was used for potassium. The concentration of each radioelement was obtained at the energy window of 1.760 MeV for eU, 1.821 MeV for eTh and 2.461 MeV for K. The concentrations were obtained using the procedure and standard calibration of IAEA (2003) and Grastly et al (1991) in Bq $kg^{-1}$. The standard radiometric units were converted to geological units using the conversion relations provided by the Polish Central Laboratory for Radiological Protection as cited by IAEA (2003), Malczewski et al., (2004) and Ogunsanwo et al. (2023). Ground concentrations, initially measured in Bq/kg, were converted to ppm (for uranium and thorium) and % (for potassium) using the conversion factors presented in Equations 1 to 3.

$$C_U(ppm) = C_U(Bq/kg) \times 0.08045 \quad (1)$$

$$C_{Th}(ppm) = C_{Th}(Bq/kg) \times 0.24331 \quad (2)$$

$$C_K(ppm) = C_K(Bq/kg) \times 0.003296 \quad (3)$$

where $C_U$ , $C_{Th}$ and $C_K$ are the concentration of $^{238}U$, $^{232}Th$ and $^{40}K$ respectively.

Integrating these methods allowed direct statistical comparison between magnetic intensity and radioelement concentrations. Regression analysis and spatial overlays demonstrated significant correlations and coincident anomaly zones, highlighting the predictive capacity of combined magnetic–radiometric interpretation for mineral exploration in mica schist terrains.

**Linear Regression Models**

In this study, three linear mathematical regression models are computed, as shown in Equations (4–6). These models represent the potential relationships between the magnetic anomaly response and each of the three radiometric parameters: uranium, thorium, and potassium, respectively.

$$M(nT) = aU_g\,(ppm) + \quad b \quad (4)$$

$$M(nT) = aTh_g\,(ppm) + \quad b \quad (5)$$

$$M(nT) = aK_g\,(\%) + \quad b \quad (6)$$

Where:

M(nT) represents the measured magnetic anomaly dataset;

Ug is the measured anomalous ground uranium concentration;

Thg is the measured anomalous ground thorium concentration;

Kg is the measured anomalous ground potassium concentration;

a and b are correction constants to be determined through regression analysis.

**Bi-Variate Statistical Analysis**

This kind of statistics was used to compare two variables having similar behaviour. In this study, Pearson product moment coefficient (PPMC) correlation and inferential statistical analysis were adopted to compare the performance of magnetic intensity and radiometric flux concentrations in the mica deposition area, J4, Ogun state.

The constructed models in Equations 4 – 6 were validated using the metric evaluation performance; namely degree of fitness and Pearson product moment correlation (PPMC) as given by Zavadzki et al (2020); Hyndman and Athanasopoulos (2021); Jadon et al (2022); Pervez and Ali (2024) in Equations 7 and 8.

$$R^2 = = 1 - \frac{\sum_{i=1}^{n}(M_i - A_i)^2}{\sum_{i=1}^{n}(M_i - \overline{A_i})^2} \quad (7)$$

$$r = \frac{n\sum M_i A_i - \sum M_i \sum A_i}{\sqrt{n\sum M_i^2 - (\sum M_i)^2}\sqrt{n\sum A_i^2 - (\sum A_i)^2}}. \quad (8)$$

where

$M_i$ is the magnetic intensity in the ith sampling point

$A_i$ is the radioelement concentration of uranium, thorium and potassium in the ith sampling points

The inferential statistics makes use of t-test as the statistical tool to validate the regression model generated for the magnetic intensity and the radioelement concentrations. The t-test formula adopted was as given in Ogunsanwo et al (2023) in Equation (9)

$$t_{n_1+n_2-2} = \frac{x_1 - x_2}{S_p{}^2\left(\frac{1}{n_1} + \frac{1}{n_2}\right)} \quad (9)$$

where,

$$S_p{}^2 = \frac{(n_1-1)S_1{}^2 + (n_2-1)S_2{}^2}{n_1+n_2-2}$$

$x_1 and x_2$ are the mean of the two samples

$S_p{}^2$ is the pooled variance

$S_1{}^2$ and $S_2{}^2$ are the variance of the two samples

$n_1 + n_2 - 2$ is the degree of freedom

$n_1$ and $n_2$ are the size of the two samples

In order to have valid conclusion on the inference obtained from the t-test analysis, the magnetic intensity and radioactive element anomalous concentrations data were subject to two sets of hypotheses as proposed by Ammar et al (1988); Youssef (2016); Ogunsanwo et al (2023)

$H_0$: There is a significant relationship between magnetic intensity and the anomalous concentrations of radioactive elements obtained from the two geological surveys (Heterogeneous).

$H_1$: There is a no significant relationship between magnetic intensity and the anomalous concentrations of radioactive elements obtained from the two geological surveys (Homogenous).

From the t-test result obtained, if the t - computed value> t-critical, the $H_1$ hypothesis is rejected, while $H_0$ is adopted. Conversely, if t- computed < t- critical, then $H_1$ hypothesis will be accepted.

**RESULTS AND DISCUSSION**

**Lithological Variation of Magnetic Intensity and Radioactive Elements in Traverse I**

The variation response to lithology of the magnetic intensity and concentration of radioactive elements (U, Th and K)

across the mica deposit area were plotted and compared as obtained in Figures 2 and 3 for traverses I and II, respectively. In traverse I, the uranium signature with that of magnetic intensity (Fig. 2a) followed similar trend from ground distance of 0 – 170m but the discrepancy set in at distance > 170m – 300 m. The peak uranium and magnetic value were obtained at the ground survey distance ranging between 120 – 140m. In between 160 – 300 ground survey distances, the magnetic intensity tend toward zero and the uranium concentration also reduces. In Figure 2b, between ground distances 80 – 160m, thorium response to lithology compare to magnetic intensity appear to follow similar trend. A very sharp anomalous low response was observed in thorium at ground distance of 60m and, relatively rises and falls in the thorium response between 170m – 300m. At 270m, the uranium and thorium concentration have the same value, which is a point of interest for further investigation along the traverse. The potassium concentration response to the lithology was observed to be above the threshold limit between the ground survey distances of 120 – 140m. The result obtained between the potassium and magnetic intensity tends to be linear at ground distance of 200 – 300 m. The ground survey distances at which peak point of all the radioactive concentration were obtained are similar. Transverse I was found to be rich in uranium concentration than thorium. Although the value obtained for the two are far above their recommended world average value of 2.8 ppm and 7.4 ppm (UNSCEAR, 2000) for uranium and thorium, respectively. Unlike potassium which only appeared to be elevated around 120 – 150 m, where the values obtained are above 1.3 % recommended world average value.

**Lithological Variation of Magnetic Intensity and Radioactive Elements in Traverse II**

In traverse II (Fig 3a), uranium concentration trend appear to exhibit linear response proximate with magnetic intensity between the ground survey distances of 5 – 165 m. A similar and elevated signature of uranium was observed around 200 – 240 m ground survey distances. Thorium concentration appears to be relatively elevated compared to uranium concentration along traverse II. The thorium concentration observed in traverse II (Fig 2b) is in equal proportion with that of traverse II (Fig 3b). Along traverse II, the thorium concentration was at its peak around horizontal ground survey distances of 5 m, 120 m, 160 m and its highest peak at 200 m. The concentration of thorium was found to attenuate between the ground distances of 260 – 300 m. The region of attenuation may be due to the permeability and porous nature of the underlying geological bedrock composition on which the traverse was conducted. The spectral variation plot indicated that thorium is more abundant in this traverse that uranium. Fig (3c) depicts the potassium concentration with the magnetic intensity response along traverse II. The result obtained reveal potassium to have its peak response around ground distance of 200 – 240 m. From all indication, uranium and potassium showcased their peak concentration around the same ground distances. The three radioelements and magnetic intensity showcased the horizontal survey distance of 200m along the traverse II as its point of interest.

Generally, the result obtained in along traverses I and II depicts that that the mica deposit area investigated have both uranium and thorium concentration in relatively high quantity. This may be attributed to the geological units such as migmatite, granodiorite and undifferentiated schist which have great tendency and ability of enhancing and elevating the uranium and thorium concentration (Masok et al 2018; Olowofela et al 2019). The reduction/ attenuation encounter around 250 -300 m. The uranium and potassium shows a good response with the magnetic intensity along the two traverses.

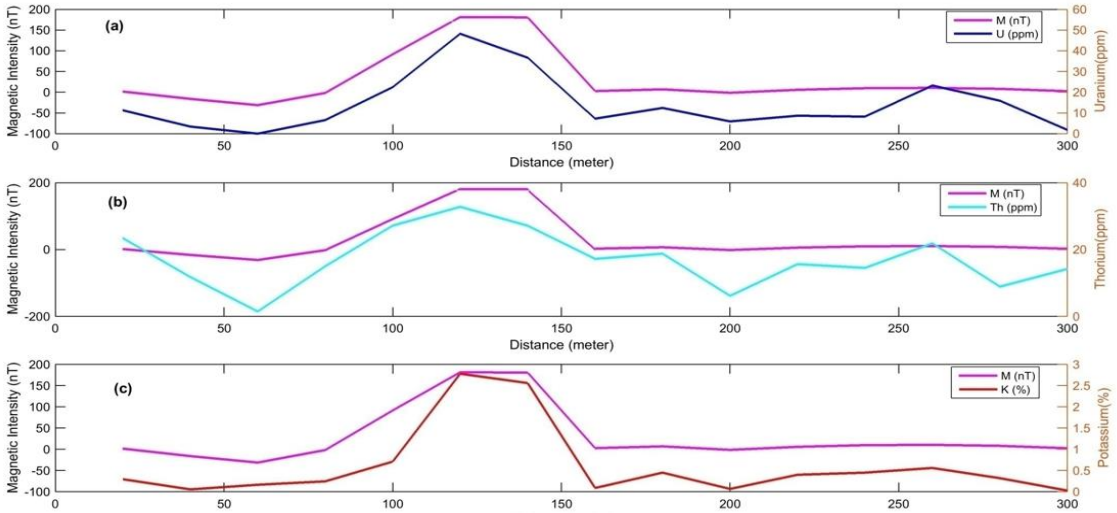


Figure 2: Spectra Variation Between Magnetic Intensity and (a) Uranium (b) Thorium (c) Potassium over the Mica Deposit Region for Traverse I

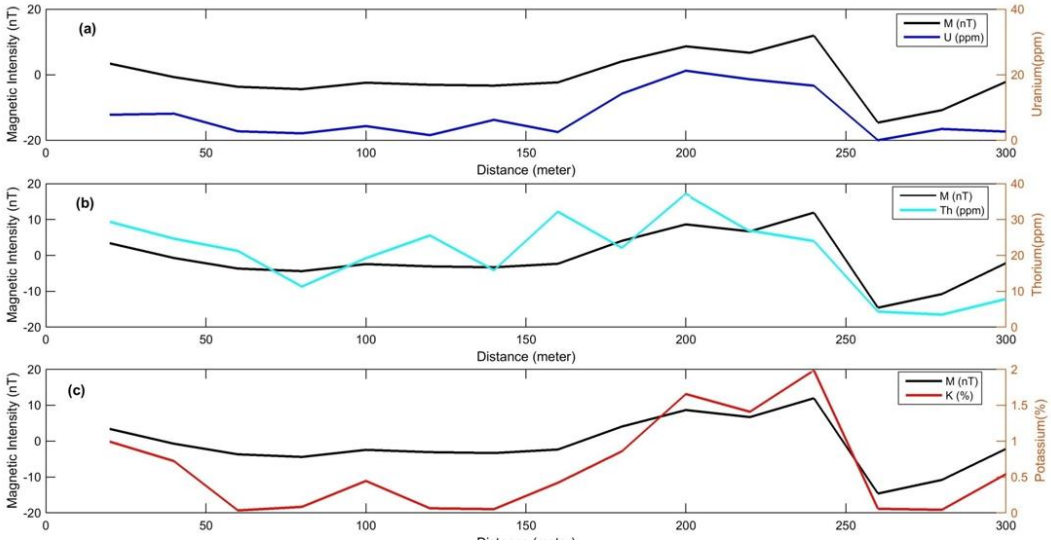


Figure 3: Spectra Variation Between Magnetic Intensity and (a) Uranium (b) Thorium (c) Potassium over the Mica Deposit Region for Traverse II

**Spatial Distribution of Magnetic Anomaly and Radioelements in Traverse I**

The 2-D visual representation of the magnetic anomaly and the three radioactive element across the two traverses were presented in Figures 4 and 5 as contour maps for traverses I and II, respectively. Figure 4a shows gridded magnetic anomalous contour map ranging from -19.964 – 113. 315 nT. The high prevalence magnetic anomaly was observed to exhibit butterfly shape pattern at the central part of the traverse I surrounded by the moderate (yellowish-green) magnetic anomaly. The elevated or strong magnetic anomalous (reddish-pink) was attributed to the granite gneiss and banded gneiss as reflect in Figure 1, while the weak magnetic anomalous response was found to be linked with the biotite composition in the North trending West and partly SE spot (blue colour).

In traverse I, the gridded uranium concentration response to the lithological composition was presented in 2D form (Fig. 4b) and its visual representation shows pattern similar to that of magnetic anomaly. The uranium concentration obtained was spatially distributed within the range of 1.126 – 29.009 ppm. The high uranium concentration spot matched with that of magnetic anomalous spot which was also linked to granite gneiss and banded gneiss. The gridded thorium spatial representation (Fig. 4c) showed that the oval spot indicating its high prevalence concentration matched with the spot for magnetic anomaly and uranium concentration. Its low concentration was assigned with biotite and eroded magmatic rock composition. The thorium spatial concentration was found to ranged between 6.020 – 24.616 ppm. The gridded potassium concentration revealed features reflecting the composite image of magnetic anomaly and uranium concentration. The potassium was found to leach out around the biotitic composition and visualised in the range of -0.082 – 1.504 %.

**Spatial Distribution of Magnetic Anomaly and Radioelements in Traverse II**

In traverse II (Fig. 5a), the gridded magnetic anomalous map showed predominantly elevate strong magnetic anomaly around banded gneiss and partly migmatite. The low concentration in the North trending Central is linked to biotite, while that at the SE corner is due to metamophorsised and eroded by hydrothermal/magmatic process leading to depletion of the crystalline migmatitic rock. The magnetic anomaly was gridded in the range of -8.585 – 8.787 nT. The gridded uranium concentration (Fig.5b) show the pattern and feature similar to that of magnetic anomaly with little discrepancy in the spot of low concentration appaears at the lower western end of high prevalence concentration and that at the NW spot of the traverse II map. The uranium concentration map was found to range between 0.525 – 18.366 ppm.

The gridded thorium (fig.5c) contour map shows low concentration pattern similar to that obtained in Fig 4a and Fig. 4c, while the highly prevalence concentration was found in the SS- SE trending to the central part of the traverse II. Thorium concentration was found to range 2.907 – 42.482 ppm. The gridded potassium contour map (Fig. 5d) shows its lower concentration at NW, SE, central part and western lineament embedded on the moderate concentration. The high prevalence concentration was found predominantly around the SS ans SE extending through the boundary to the upper central part of the contour map. The concentration was found to range between 0.034 – 1.551 %.

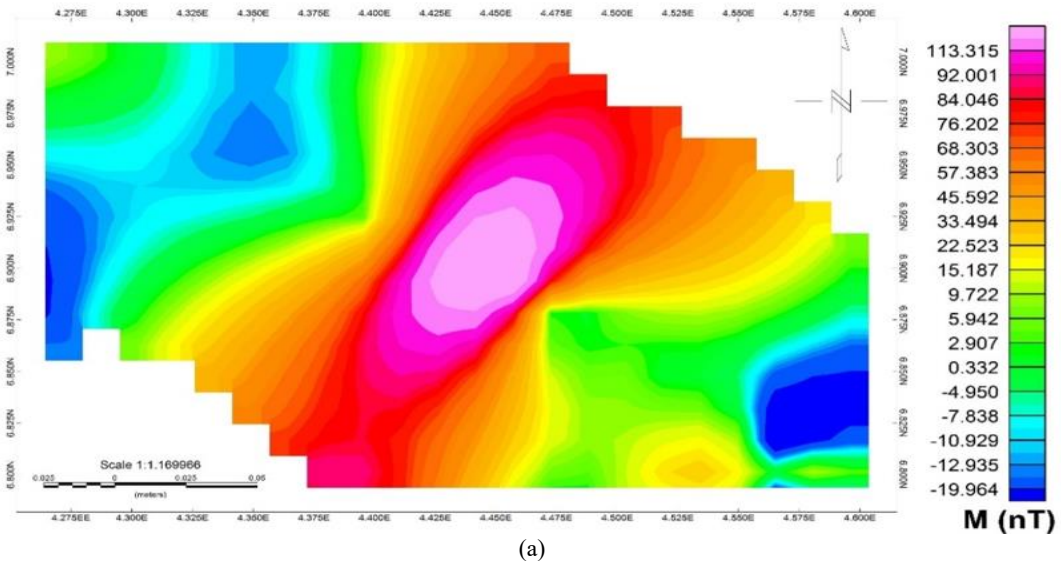
113.315
92.001
84.046
76.202
68.303
57.383
45.592
33.494
22.523
15.187
9.722
5.942
2.907
0.332
-4.950
-7.838
-10.929
-12.935
-19.964
M (nT)
Scale 1:1.169966

(a)

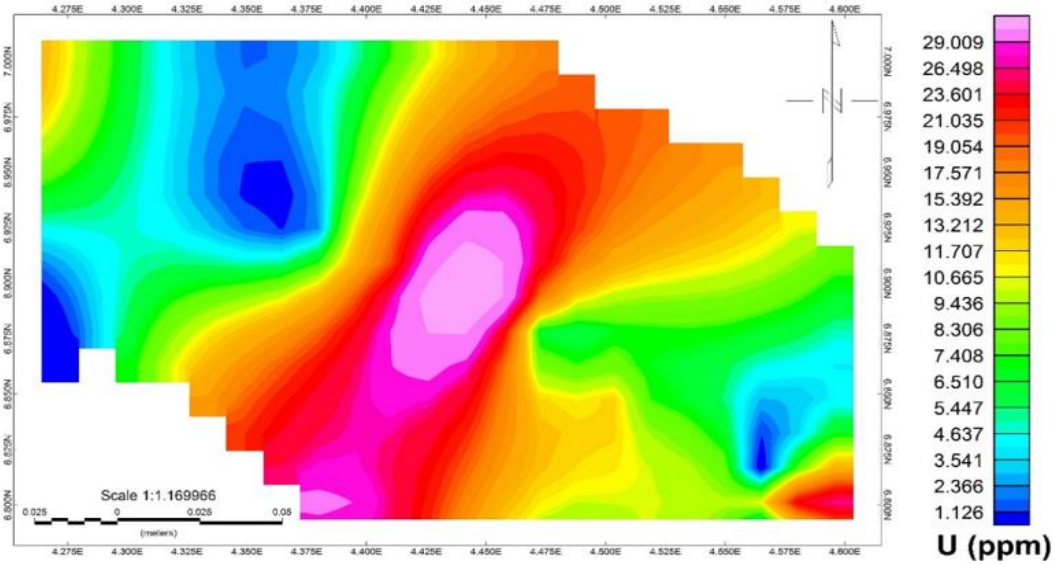
29.009
26.498
23.601
21.035
19.054
17.571
15.392
13.212
11.707
10.665
9.436
8.306
7.408
6.510
5.447
4.637
3.541
2.366
1.126
U (ppm)
Scale 1:1.169966

(b)

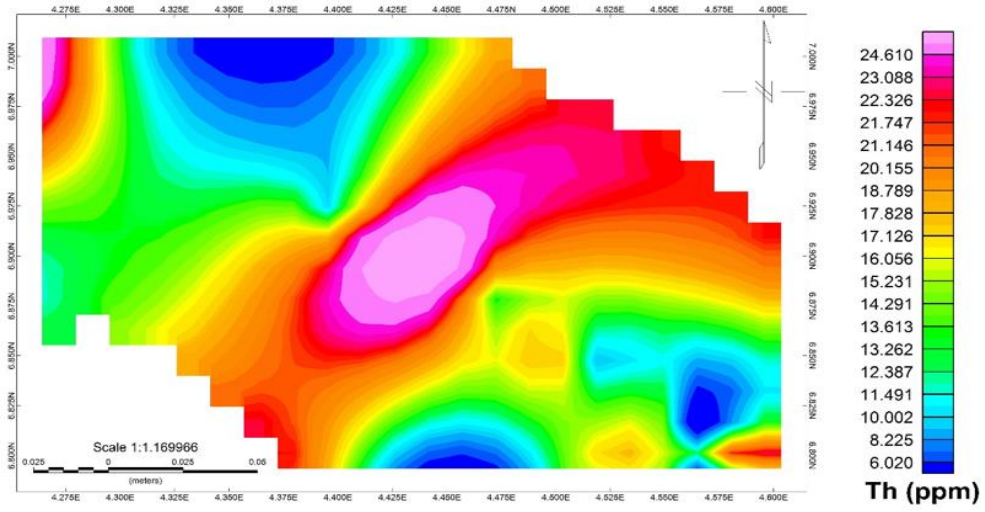
24.610
23.088
22.326
21.747
21.146
20.155
18.789
17.828
17.126
16.056
15.231
14.291
13.613
13.262
12.387
11.491
10.002
8.225
6.020
Th (ppm)
Scale 1:1.169966

(c)

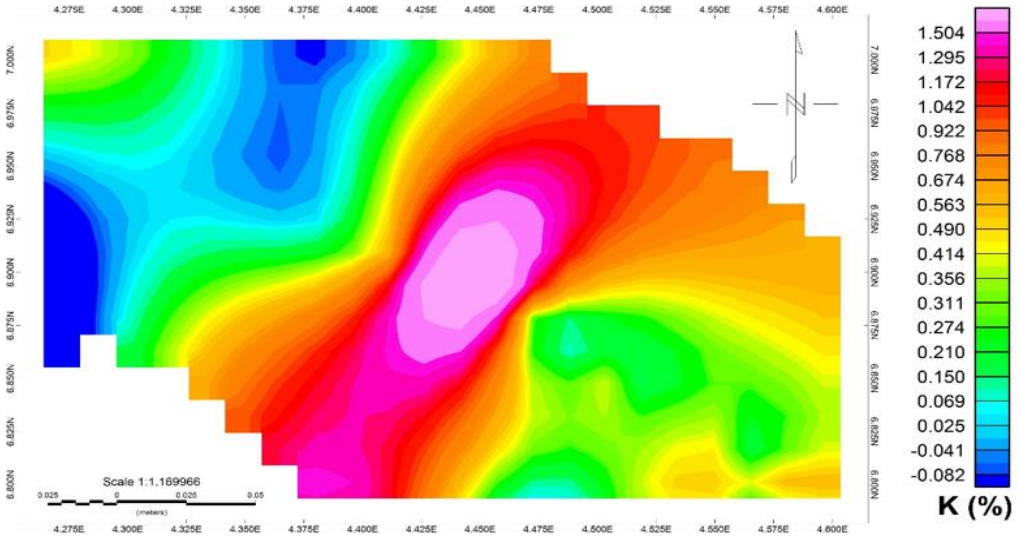


(d)

Figure 4: Spatial distribution of (a) Magnetic anomaly (b) uranium concentration (c) Thorium concentration (d) Potassium concentration in Traverse I

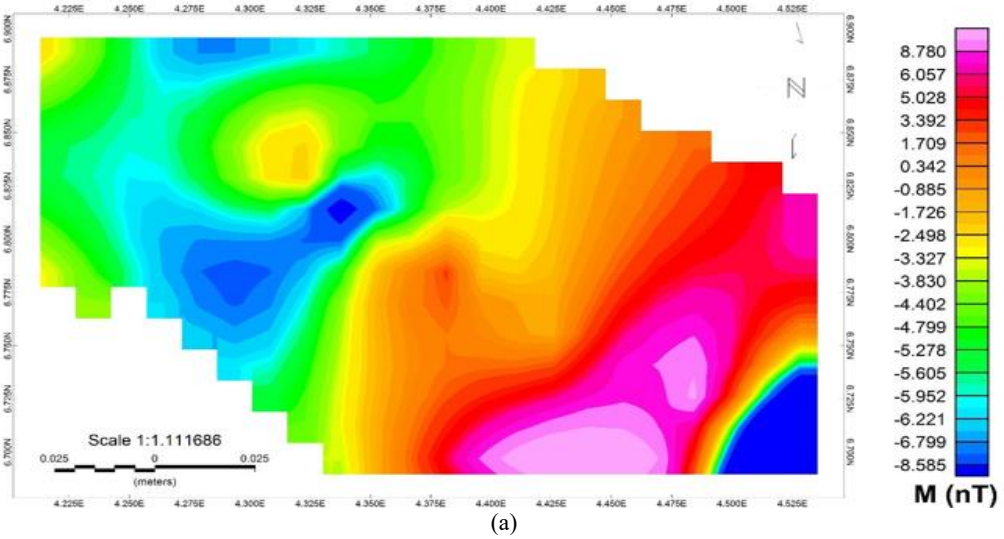


(a)

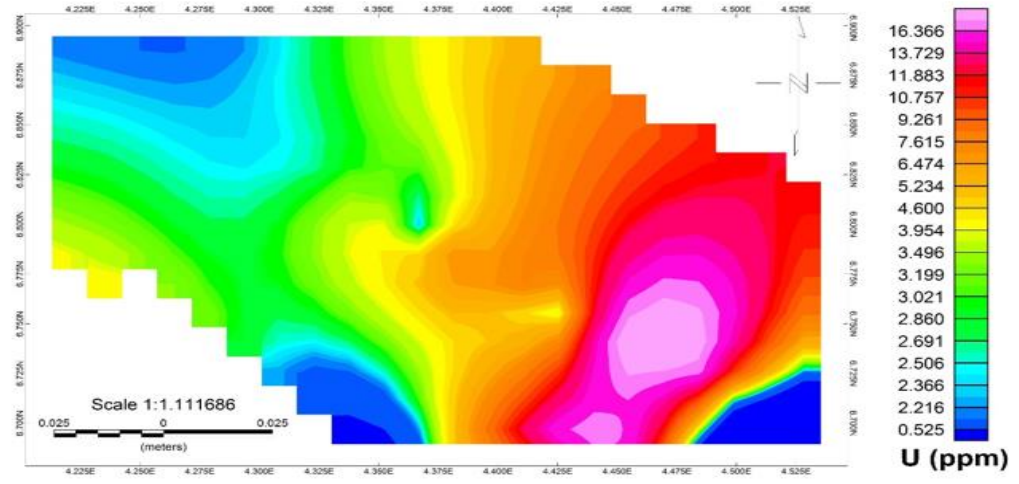


(b)

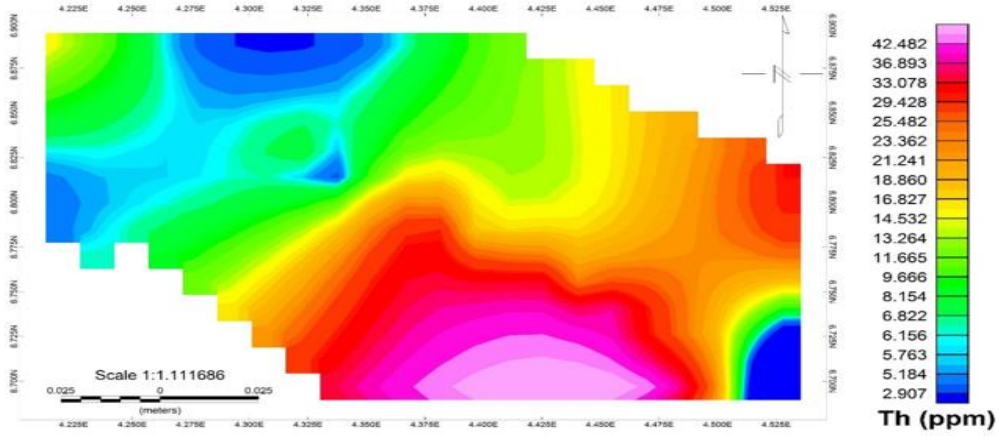


(c)

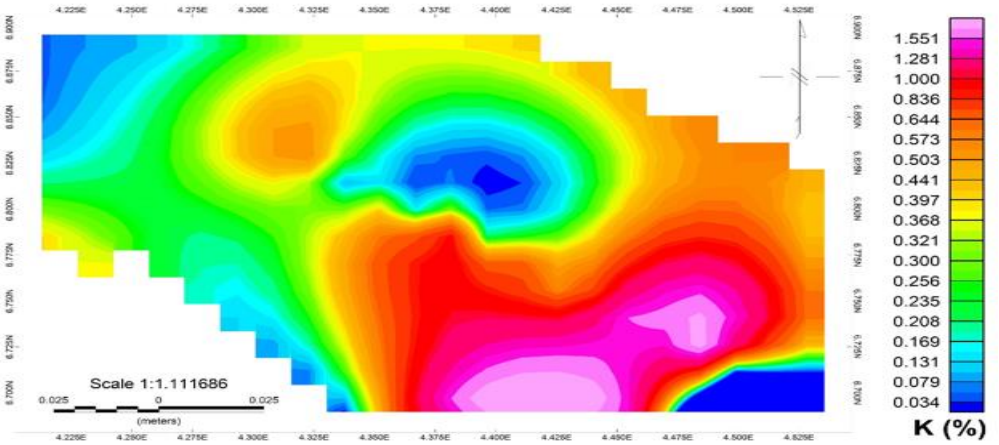


(d)

Figure 5: Spatial Distribution of (a) Magnetic Anomaly (b) Uranium Concentration (c) Thorium Concentration (d) Potassium Concentration in Traverse II

**Geological Implications**

The spatial coincidence of thorium, uranium, and magnetic anomalies suggests a strong lithological and mineralogical control on radioelement distribution in the study area. Thorium and uranium often occur together in accessory minerals such as monazite, zircon, allanite, and xenotime, which are typically concentrated in felsic pegmatites, mica schists, or zones of hydrothermal alteration. Their alignment with magnetic anomalies indicates that the same structural or lithological features responsible for enhanced magnetization (magnetite or ilmenite-bearing horizons, pegmatitic intrusions) are also the loci of radioelement enrichment. This spatial association implies that structural controls such as faults, shear zones, or lithological contacts may serve as conduits for mineralizing fluids or as sites of accessory mineral accumulation.

The potassium distribution, on the other hand, showing a composite relationship with both uranium and magnetic anomalies, reflects its dual role. Potassium is commonly hosted in K-feldspar, biotite, and muscovite—minerals abundant in mica schists and pegmatites. Its spatial overlap with uranium anomalies may indicate hydrothermal K-metasomatism, where uranium mineralization is accompanied by potassic alteration. The partial alignment with magnetic anomalies suggests that potassium-bearing minerals also contribute to the lithological framework associated with magnetic sources.

In geological terms, these spatial patterns point to a inherent link between magnetic mineral assemblages and radioelement-bearing phases, likely controlled by the tectonothermal history of the mica schist terrain. The overlapping anomalies delineate prospective zones for radioelement-associated mineralization, particularly pegmatite-hosted U–Th mineralization with potassic alteration halos.

**Estimated Models**

In this study, the composite linear regression models relating the magnetic intensity or magnetic power density to the radioelements were established using scattered plot (Figure 6) after the normalization procedure had been conducted**.** The equation which satisfied the proposed empirical models was as presented in Equations (10 – 12) for magnetic intensity against uranium, thorium and potassium respectively.

The composite linear regression model of magnetic intensity to uranium concentration was as obtained in Equation 10.

$$M = 3.88\,U - 27.39 \quad (10)$$

The composite linear regression model of magnetic intensity to thorium concentration was as obtained in Equation 11.

$$M = 2.45\,Th - 31.31 \quad (11)$$

The composite linear regression model of magnetic intensity to potassium concentration was as obtained in Equation 12.

$$M = 51.04\,K - 16.92. \quad (12)$$

The linear models generated from the composite regression analysis of magnetic intensity data alongside the radioactive elements show the reflection of positive slope. Theoretically, the result obtained implies that the magnetic intensity has

direct proportion relation with the radioactive elements across the study area.

Empirically, the linear fit result has proven the fact that the magnetic intensity of the The composite uranium concentration accounted highest degree of fitness ($R^2$) value of 0.76 with the magnetic intensity. The composite thorium concentration accounted for $R^2$ value of 0.40 with the magnetic intensity, while composite potassium concentration revealed the $R^2$ value of 0.40 with the magnetic intensity study area is in good agreement with geological response of the study area. This implies that the undifferentiated schist which has been identified as mica-quartz schist has strong affinity for both the magnetic intensity and radio element concentrations in the study area. The magnetic intensity having responded well to the bedrock composition and varies directly with radio element concentrations revealed that the high region of magnetic intensity in the mica deposit area will be in consonance with the zone of radioelement high prevalence and vice versa.

The statistical relationships established between magnetic intensity and radioelement concentrations provide important guidance for mineral exploration within the mica schist terrain of Ogun State. The strong correlation between uranium concentration and magnetic anomalies ($R^2 = 0.76$) highlights uranium as the most reliable geochemical indicator for targeting mineralization in this setting. The close association suggests that uranium-bearing accessory minerals are structurally and lithologically linked to magnetite- or ilmenite-bearing horizons and migmatitic bodies within the schist. Consequently, integrated mapping of uranium and magnetic highs can be used as a predictive tool to delineate prospective zones for uranium- and pegmatite-related mineralization.

The moderate correlations of thorium and potassium ($R^2 = 0.40$ each) suggest that while these elements are spatially associated with magnetic features, their distributions are influenced by additional geological factors. Thorium, commonly hosted in resistant phases such as monazite, may be dispersed along structural fabrics but not consistently tied to magnetic mineralization. Potassium anomalies, by contrast, likely reflect potassic alteration halos associated with hydrothermal processes, which may partially overlap with uranium-rich zones but also extend into non-magnetic schist units. As such, thorium and potassium data provide valuable secondary information, enhancing anomaly characterization when interpreted alongside uranium–magnetic associations.

Geologically, these results imply that uranium mineralization in the mica schist belt is more predictably associated with magnetic anomalies than either thorium or potassium. Thus, uranium serves as the most reliable radioelemental indicator when integrated with magnetic surveys for targeting mineralization in this terrain, while thorium and potassium provide complementary but less deterministic signatures.

For exploration strategy, this implies that uranium anomalies co-located with magnetic highs should be prioritized as primary targets, while thorium and potassium signatures serve to refine interpretations and detect alteration footprints. The combined approach reduces ambiguity, increases predictive confidence, and supports more efficient prospecting within structurally complex Precambrian schist belts.

**Models Performance Validation**

The linear models performance between the magnetic intensity and the radioelements were validated using the person product moment correlation analysis and inferential t-test statistical analysis. Inferential statistics are primarily used to validate relationships between two or more variables (Hou et al., 2021; Fotheringham et al., 2024). In this study, a t-test was employed to assess the relationship between magnetic flux and radiometric flux across the study area at 95 % confidence level. This analysis was necessary to confirm the established associations between magnetic intensity and the concentrations of radioelements.

The results for the three radioelements and magnetic intensity across the two traverses indicate no significant difference between them. Specifically, the calculated t-values were less than the critical value (as shown in Table 1), and the corresponding p-values were all greater than 0.05. This implies that the null hypothesis ($H_0$) was rejected, and the alternative hypothesis ($H_1$) was accepted, thereby supporting the existence of a statistically significant relationship between magnetic intensity and radioelement concentrations.

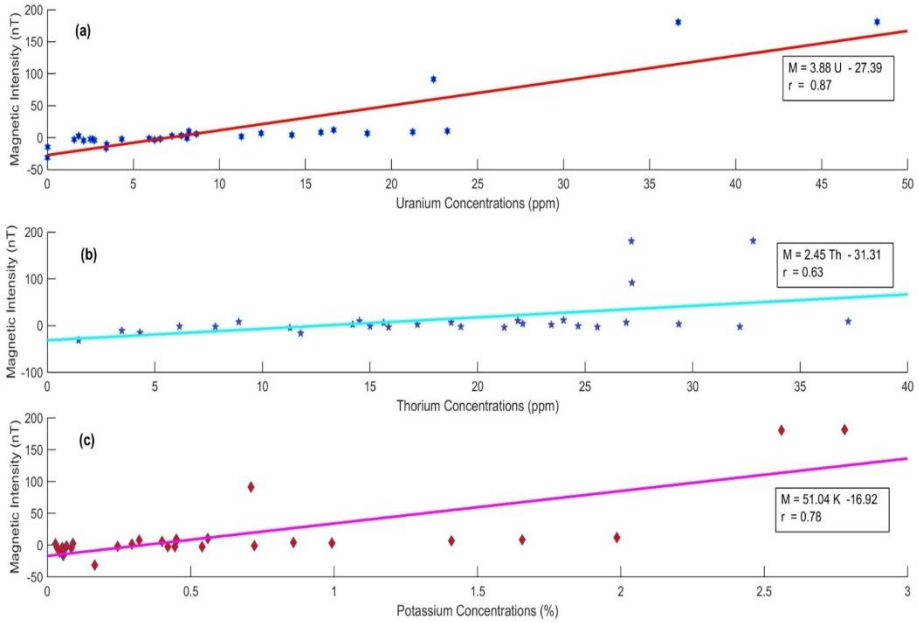


Figure 6: Composite Linear Relation Between the Magnetic Intensity and the Radioactive Elements Concentration

**Table 1: Summary of t – test Inferential Statistics**

| | Survey parameters | t-calculated | t-critical | p-value | r-value |
|---|---|---|---|---|---|
| **Traverse 1** | M – U | 0.91 | 2.04 | 0.37 | 0.93 |
| | M – Th | 0.75 | 2.04 | 0.45 | 0.78 |
| | M – K | 1.75 | 2.04 | 0.09 | 0.96 |
| **Traverse 2** | M – U | -3.29 | 2.04 | 0.02 | 0.86 |
| | M – Th | -6.71 | 2.04 | 0.05 | 0.74 |
| | M – K | -0.82 | 2.04 | 0.42 | 0.90 |

The t-calculated indicate negative values at traverse 2 while the values obtained in traverse 1 are positive. The findings indicate that the regression models incorporating uranium and potassium concentrations with magnetic intensity across the two traverses exhibit greater statistical reliability. The lithological responses between the magnetic intensity and all the radioelement analysed revealed a very strong coefficient along the two traverses in the mica deposits area. The variability of the models across different areas reflects the influence of underlying bedrock composition. In this study, the regression models demonstrated a stronger fit for uranium and potassium than for thorium.

## CONCLUSION

This study demonstrates the significance of integrating magnetic and radiometric methods in the investigation of mica schist terrains, a context where such joint applications have received limited attention. By combining proton precession magnetometer measurements with sodium iodide (NaI) gamma spectrometry, the research captures both the magnetization contrasts and radioelement (U, Th, K) concentrations across the mica deposit zone of Area J4, Ogun State, Nigeria. The integration revealed strong positive correlations, with uranium showing the highest degree of fit with magnetic intensity, followed by thorium and potassium. Regression analyses confirmed direct proportional relationships, thereby establishing a predictive framework in which anomalies detected in one dataset can be inferred or validated through the other.

The spatial coincidence of magnetic anomalies with uranium- and thorium-enriched zones further highlights the geological significance of integrating datasets, pointing to radioelement-associated mineralization potential within the schist belt. These results demonstrate that empirical relationships between magnetic and radiometric signatures reduce interpretational ambiguities and enhance the reliability of anomaly discrimination. This strengthens mineral exploration efficiency, particularly in geologically complex Precambrian settings where single-method surveys may miss subtle but economically relevant targets.

Beyond the local implications, this study emphazise the wider applicability of integrating multiple geophysical methods for resource exploration and geological mapping. Although constrained by limited survey coverage and the focus on near-surface soil samples, the results lay a foundation for broader-scale investigations and deeper subsurface characterization. Conclusively, the integration of magnetic and radiometric datasets is shown to provide a scientifically rigorous and practically valuable framework for predictive mineral targeting within mica-rich terrains.

## ACKNOWLEDGEMENT

The authors wish to thank and appreciate the people of Area J4, for their support in making the research realisable.

## REFERENCES

Abdus-Salam, M., Bolarinwa, A., Olatunji, A., Fullen, M., Afolabi, A., Omotunde, V., Olajide-Kayode, J., and Olisa, O. (2020). Geochemistry and mineral chemistry of quartz mica schists within Iseyin-Oyan Schist Belt, South-Western Nigeria. *Indian Journal of Science and Technology, 13*(41): 4319–4331. https://doi.org/10.17485/IJST/v13i41.1628

Airo, M. L. (2007). Application of aerogeophysical data for gold exploration: Implications for the central Lapland greenstone belt. In V. J. Ojala (Ed.), *Gold in the Central Lapland Greenstone Belt* (pp. 171–192). Geological Survey of Finland.

Alaku, O. I., Moshood, I. O., Agbor, T. A., and Amos, A. A. (2017). Geochemical characteristics and petrogenesis of Malumfashi Schist around Tandama area, north-western Nigeria. *British Journal of Applied Science & Technology, 20*(1): 1–14. https://doi.org/10.9734/BJAST/2017/30116

Ammar, A. A., Abdelhady, H. M., Soliman, S. A., and Sadek, H. S. (1988). Aerial radioactivity of phosphate in the western central eastern desert of Egypt. *Earth Sciences, 1*(1): 181–203. https://doi.org/10.4197/EAR.1-1.10

Ammar, A. A., El Sirafe, A. M., and El Kattan, E. M. (1993). Airborne geochemical and structural investigation of the Precambrian copper-bearing rocks, Hammash District, Southeastern Desert, Egypt. *Annals of the Geological Survey of Egypt, 19*: 467–486.

Ayanda, J. D., Badmus, B. S., and Popoola, I. O. (2006). Geoelectric evaluation of mica deposits in Area J4 of South-West Nigeria. *Journal of Applied Science and Technology, 11*(1–2): 39–43. http://ajol.info/index.php/just/article/view/

Ayanda, J. D., and Popoola, I. O. (2018). Geoelectrical exploration for groundwater potential and basement terrain in parts of Area J4 Southwest Nigeria. *TASUED Journal of Pure and Applied Science, 1*(1): 387–394.

Beamish, D. (2013). Gamma ray attenuation in the soil of Northern Ireland, with special reference to peat. *Journal of Environmental Radioactivity, 115*: 13–27. https://doi.org/10.1016/j.jenvrad.2012.05.031

Blakely, R. J. (1995). *Potential theory in gravity and magnetic applications*. Cambridge University Press. https://doi.org/10.1017/CBO9780511549816

Boadi, B., Wemegah, D. D., and Preko, K. (2013). Geological and structural interpretation of the Konongo area of the Ashanti gold belt of Ghana from aeromagnetic and radiometric data. *International Research Journal of Geology and Mining, 3*(3): 124–135. http://www.interesjournals.org/IRJGM

Dickson, B. L., and Scott, K. M. (1997). Interpretation of aerial gamma-ray surveys: Adding the geochemical factors. *AGSO Journal of Australian Geology and Geophysics, 17*(2), 187–200.

Elhusseiny, A. A. (2022). Integrated structure and mineralization study using aeromagnetic, aerospectrometric and remote sensing data at Esh El-Mallaha area, Eastern Desert, Egypt. *Geomaterials, 13*(1): 1–22. https://doi.org/10.4236/gm.2023.131001

El-Sadek, M. A. (2002). Application of thorium-normalized airborne radiospectrometric survey data of Wadi Araba area, Northeastern Desert, Egypt, as a guide to the recognition of probable subsurface petroleum accumulations. *Applied Radiation and Isotopes, 57*(1): 121–130. https://doi.org/10.1016/S0969-8043(02)00082-9

Fotheringham, A. S., Oshan, T. M., and Li, Z. (2024). *Multiscale geographically weighted regression: Theory and practice*. CRC Press. https://doi.org/10.1201/9781003435464

Fouad, K. M. (1996). Synoptic view of the different domains of application of airborne radiometric and spectrometric surveys in Egypt. In *Proceedings of the Third Conference on the Peaceful Uses of Atomic Energy* (pp. 185–212). Damascus, Syria.

Grasty, R. L., Holman, P. B., and Blanchard, Y. B. (1991). Transportable calibration pads for ground and airborne gamma-ray spectrometers. *Geological Survey of Canada, Paper 90-23,* 25 p. https://doi.org/10.4095/132237

Hinze, W. J., von Frese, R. R. B., and Saad, A. H. (2013). *Gravity and magnetic exploration: Principles, practices, and applications*. Cambridge University Press. https://doi.org/10.1017/CBO9780511843129

Hou, K., Mo, H., Xue, C., and Zhang, L. (2021). An augmented q-factor model with expected growth. *Review of Finance, 25*(1): 1–41. https://doi.org/10.1093/rof/rfaa004

Hyndman, R. J., and Athanasopoulos, G. (2021). *Forecasting: Principles and practice* (3rd ed.). OTexts. https://otexts.com/fpp3/

International Atomic Energy Agency (IAEA). (2003). *Guidelines for radioelement mapping using gamma-ray spectrometry data* (IAEA-TECDOC-1363). IAEA.

Jadon, A., Patil, A., and Jadon, S. (2022). A comprehensive survey of regression-based loss functions for time series forecasting. *arXiv Preprint, arXiv:2211.02989*, 13. https://doi.org/10.48550/arXiv.2211.02989

Malczewski, D., Taper, L., and Dorda, J. (2004). Assessment of natural and anthropogenic radioactivity levels in rocks and soils in the environs of Swieradow Zdroj in Sudetes, Poland, by in situ gamma-ray spectrometry. *Journal of Environmental Radioactivity, 73*(3): 233–245. https://doi.org/10.1016/j.jenvrad.2003.08.010

Masok, F. B., Masiteng, P. L., Mavunda, R. D., Maleka, P. P., and Winkler, H. (2018). Measurement of radioactivity concentration in soil samples around phosphate rock storage facility in Richards Bay, South Africa. *Journal of Radiation Research and Applied Sciences, 11*(1): 29–36. https://doi.org/10.1016/j.jrras.2017.10.006

Minty, B. R. S. (1997). Fundamentals of airborne gamma-ray spectrometry. *AGSO Journal of Australian Geology and Geophysics, 17*(2), 39–50.

Odokuma-Alonge, O., and Dibani, S. C. (2022). Geochemical and petrographic studies of some quartz mica schists in Igarra and environs, South-Western Nigeria. *International Journal of Earth Science Knowledge and Applications, 4*(3): 476–485. http://www.ijeska.com/index.php/ijeska

Ogunsanwo, F. O., Ayanda, J. D., Mustapha, A. O., Olatunji, A. T., Ozebo, V. C., Olurin, O. T., Alaka, A. O., Okeyode, I. C., Adepitan, J. O., and Olowofela, J. A. (2023). Empirical relation between magnetic and radiometric survey in bitumen area, Ogun State, Nigeria. *RMZ–Materials and Geoenvironment, 69*(2): 1–14. https://doi.org/10.2478/rmzmag-2023-0003

Ohioma, J. O., Ezomo, F. O., and Akinsunmade, A. (2017). Delineation of hydrothermally altered zones that favour gold mineralization in Isanlu area, Nigeria using aeroradiometric data. *International Journal of Applied Science, 2*(1): 20–27. https://doi.org/10.21467/ias.2.1.20-27

Olowofela, J. A., Okeyode, I. C., Idowu, O. A., Olurin, O. T., and Ogunsanwo, F. O. (2019). Lithological mapping of Ogun State, Southwestern Nigeria, using aeroradiospectrometry. *Environmental Earth Sciences, 78*(7): 263. https://doi.org/10.1007/s12665-019-8256-6

Pervez, A., and Ali, I. (2024). Robust regression analysis in analyzing financial performance of public sector banks: A case study of India. *Annals of Data Science, 11*(1): 677–691. https://doi.org/10.1007/s40745-022-00427-3

Ramadass, G., SubhashBabu, A., and Udaya, L. G. (2015). Structural analysis of airborne radiometric data for identification of kimberlites in parts of Eastern Dharwar Craton. *International Journal of Science and Research, 4*(4): 2379–2380.

Shirazy, A., Ziaii, M., Hezarkhani, A., and Timkin, T. (2020). Geostatistical and remote sensing studies to identify high metallogenic potential regions in the Kivi area of Iran. *Minerals, 10*(10): 869. https://doi.org/10.3390/min10100869

Saunders, D. F., Burson, K. R., Branch, J. F., and Thompson, C. K. (1993). Relation of thorium-normalized surface and aerial radiometric data to subsurface petroleum accumulations. *Geophysics, 58*(10): 1417–1427. https://doi.org/10.1190/1.1443357

United Nations Scientific Committee on the Effects of Atomic Radiation (UNSCEAR). (2000). *Exposure from natural radiation sources* (Annex B). United Nations.

Usman, M. A., and Ibrahim, A. A. (2017). Petrography and geochemistry of rocks of Northern part of Wonaka Schist Belt, Northwestern Nigeria. *Nigerian Journal of Basic and Applied Science, 25*(2): 87–99.

Youssef, M. A. S. (2016). Relationships between ground and airborne gamma-ray spectrometric survey data, North Ras Millan, Southern Sinai Peninsula, Egypt. *Journal of Environmental Radioactivity, 152*, 75–84. https://doi.org/10.1016/j.jenvrad.2015.09.008

Zavadzki, T., de Pauli, S., Kleina, M., and Bonat, W. H. (2020). Comparing artificial neural network architectures for Brazilian stock market prediction. *Annals of Data Science, 7*(3): 613–628. https://doi.org/10.1007/s40745-020-00305-w

©2025 This is an Open Access article distributed under the terms of the Creative Commons Attribution 4.0 International license viewed via https://creativecommons.org/licenses/by/4.0/ which permits unrestricted use, distribution, and reproduction in any medium, provided the original work is cited appropriately.